Journal of the European Ceramic Society **18** (1998) 595–600

PII: S0955-2219(97)00207-0
0955-2219/98/$19.00 + 0.00

Grain-boundary Grooves and Surface Diffusion in Polycrystalline Alumina Measured by Atomic Force Microscope

Woosuck Shin, Won-Seon Seo and Kunihito Koumoto*

Department of Applied Chemistry, Graduate School of Engineering, Nagoya University, Furo-cho, Chikusa-ku, Nagoya 464-8603, Japan

(Received 22 October 1997; revised version received 00 Month Year; accepted 20 November 1997)

Abstract

Grain-boundary grooving was studied on polished surfaces of polycrystalline alumina, after it was annealed at 1370~1600°C in air. The groove angles and the groove widths were measured by AFM and it was determined that surface diffusion is the dominant mechanism for the mass transport and the ratio of grain-boundary energy to surface energy decreased with increasing temperature. The surface diffusion coefficient calculated was $D_s = 8{\cdot}22 \times 10^7 \times exp[-577 \pm 30(kJ\,mol^{-1})/RT]$ *which is the smallest among those reported in the literature.* © *1998 Elsevier Science Limited. All rights reserved*

1 Introduction

Distributions of grain-boundary dihedral angles and groove profiles which can reveal the kinetics of changes in topography of ceramic surfaces under capillary force have been measured in the past several decades.[1–5] The information on grain-boundary energy, surface energy and the kinetics of the mass transport is important in understanding of various phenomena, such as fracture, sintering, grain growth, etc. Thermal grooving has been known as one of the most useful methods to study the change in the ratio of grain-boundary energy to surface energy and the mass transport on ceramic surfaces (Fig. 1), since by the help of the well-known theory developed by Mullins[6] the grain-boundary grooving can be evaluated analytically. According to Mullins theory the linear dimension of groove profile, i.e. the groove width w, increases uniformly with time t when the grain-boundary grooving proceeds by surface diffusion:

$$w = 4{\cdot}6(Bt)^{1/4} \tag{1}$$

where

$$B = D_s \delta \sigma_{SV} \Omega / kT \tag{2}$$

in which D_s is the surface diffusion coefficient, δ the thickness of surface layer, σ_{SV} the free energy of the solid–gas interface, Ω the molar volume of diffusing species, k the Boltzmann constant and T the absolute temperature.

The purpose of this work was to determine if we could measure the groove angles and profiles in polycrystalline alumina by use of atomic force microscope (AFM) as a scanning profilometer. AFM is capable of investigating the surface of an insulator at an atomic scale and has a higher resolution[7] (maximum lateral resolution: 0·2 nm, vertical resolution: 0·01 nm) than any other technique, such as the Carbon or Metal Reference Line (CMR, MLR) technique and Optical Interferometry (OI).[8] OI was also attempted in this study. However, because the resolution determined by the wave length of the light used and the numerical aperture was poor and the grooves developed by thermal etching were too small to be measured accurately, the results could not be included in this paper.

2 Experimental Procedure

A high density (99·9%) polycrystalline alumina (Nippon Kagaku Togyo, Al_2O_3 99·76, SiO_2 0·08, MgO 0·06, Na_2O 0·05, CaO 0·04, Fe_2O_3 0·01 wt%) was cut with a diamond saw into small rectangular plates ($3 \times 3 \times 2\,mm^3$) and they were polished to final finish by 1/4 μm diamond abrasive grains. The sample was placed in an alumina boat and

*To whom correspondence should be addressed.

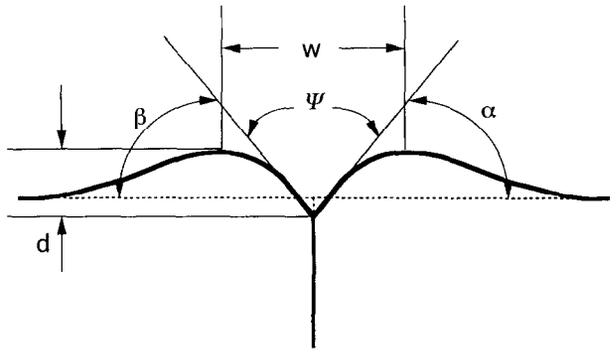

Fig. 1. Schematic cross-sectional view of a grain-boundary groove.

annealed at 1370~1600°C in air in an alumina reaction tube. Alumina boats and reaction tubes of high purity and quality similar to the sample were employed for annealing so that impurity pick-up during annealing might be minimized. The groove profile was analyzed from the surface images obtained by AFM(Atomic Force Microscope; Seiko Electronic. Co., SFA300). Scanned area ($10\times10\,\mu m^2$ for large, $2\times2\,\mu m^2$ for smallest groove) showed several grain boundaries and then a line vertical to the grain boundary was drawn to measure the cross-sectional profile of the groove. The dihedral angle, Ψ_s, the groove width, w, and the groove depth, d, were directly read via the profile of this line (Fig. 2). The measurement of the groove was made for over 25 different grain-boundaries in every one sample. The dihedral angle also was calculated from the dimension of the quasi-static groove profile formed by surface diffusion using the Mullins equation.

$$\Psi_s = 180 - 2\ \tan^{-1}(d/0{\cdot}21\ w) \qquad (3)$$

The constant force mode was employed in AFM imaging and over 25 grain boundaries were analyzed for every sample. The sensitivity was about 30×10^{-9} N/nm and controlled to be small as the surface roughness increased with increasing annealing temperature.

3 Results and Discussion

3.1 Groove profiles and accuracy of AFM measurement

The cantilever of AFM is made of a thin film silicon nitride and a small tip with pyramid shape is grown at its end by CVD. The angle of this tip is 70° determined by the two planes of the Si (111) and (1$\bar{1}$1). For small grooves, the rounded end of this tip with the diameter of 50 nm can affect the resolution of AFM.

When we scan the surfaces, the sides of the grain boundaries are almost always asymmetric. The dihedral angle is obtained from the sum of the inclination angles of both sides and the depth was obtained as the mean value of two different distances between maximum point and minimum point. The groove angle was measured using two tangential lines on the groove profile drawn along the linear inclination region(at about 5–10% of the groove width away from the center of the groove for all samples, $\Psi = 180\text{-}\alpha\ \text{-}\beta$, see Fig. 3). The measurement of the angle was done at the point as close as possible to the center of the groove. In the center of the groove, the measured data are unreliable because the end of the tip of the cantilever has a radius of 25 nm.

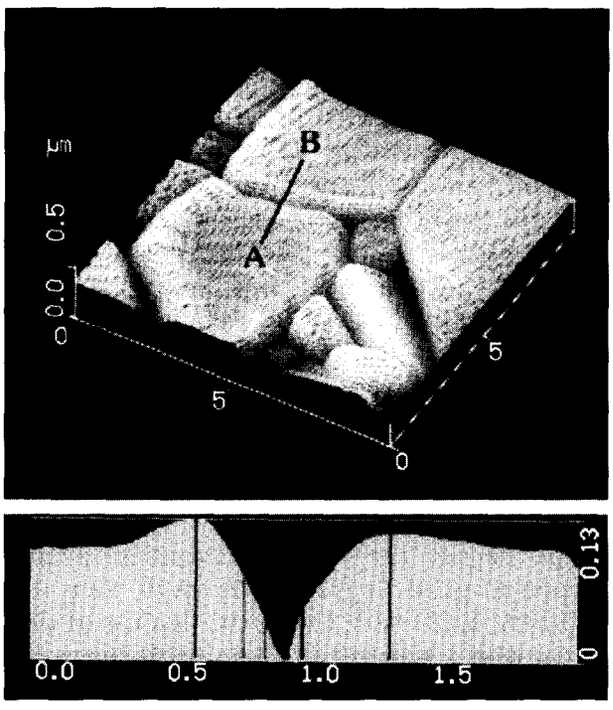

Fig. 2. AFM image of the surface of the alumina with a cross-sectional view of A–B line; $T = 1530$°C, $t = 1$ h.

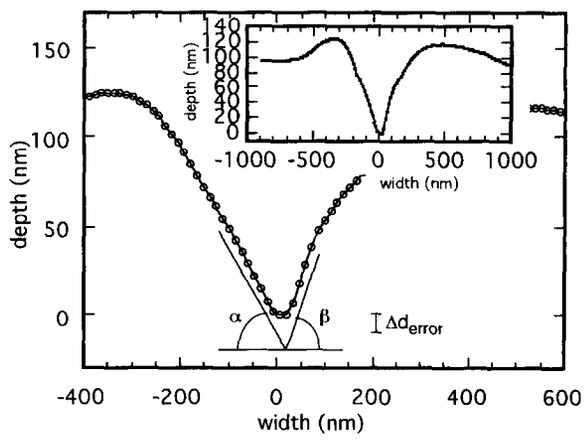

Fig. 3. Profile of the center of the groove shown in Fig. 2 showing the error of the depth due to AFM tip (insert shows entire groove profile).

If the surface of the sample is scanned with small span, the spatial resolution will increase up to the resolution of the AFM itself of a few Angstrom. For instance, a $2\,\mu m \times 2\,\mu m$ scan would give data point every 4 nm and the maximum error obtainable for diagonal direction would be 5·6 nm and $1\,\mu m \times 1\,\mu m$ would give the maximum error of 2·8 nm. However, for the dihedral angle measurement, the measurement errors can come from small grooves or grooves of small dihedral angles, because the tip of AFM has a radius of 25 nm and has a cone angle of 70° in the case of this paper.[9] This tip artifact made the measured groove profile rounded in the center of the groove and the width of the rounded region is around 30 nm for almost all of the samples measured in this study. This is of the same order as the expected maximum error of 18 nm ($18 = 25 \times \sin 45°$) comes from the shape of tip. The resulting error of the depth, Δd_{error} is expected to be around 10 nm but not considered in the following analysis for simplicity. However, the accuracy of the dihedral angle measurements would be bad at the small grooves because these errors do not become smaller when grooves become small. Considering this Δd_{error} the difference between measured Ψ by the tangential lines and the calculated one from eqn (3) would be much larger as the groove becomes smaller. Although the most small grooves measured also showed the linear inclination regions usable for the Ψ measurement, these tip artifacts would also introduce considerable error when the groove dimension becomes smaller.

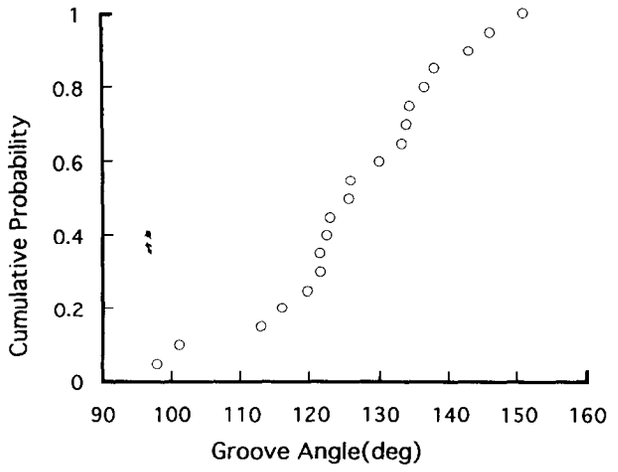

Fig. 4. Cumulative probability of the groove angles; $T = 1450°C$, $t = 4$ h.

3.2 Groove angles

Generally, the surface free energy of alumina can be assumed to be independent of orientation for all practical purposes.[10] Another assumption can also be made that the relative grain-boundary energy (σ_b/σ_{SV}) is constant for a wide range of misorientation angles based on other workers' experimental reports.[10] Since it is not possible to see if the observed grain boundaries are perpendicular to polished surface or not, the statistical distributions of the angles are usually presented as shown in Fig. 4. It is difficult to show all the distributions of Ψ for every sample but the S-shaped distributions were observed for all the samples. The observed distributions are summarized in Table 1 with the average values compared with other reported values in Table 2. The difference between the minimum and the maximum values of each Ψ measurement is in the range of 31 to 61° and similar to the values reported by others. From the groove depth, d, and the groove width, w, the dihedral angle can be calculated using eqn (3). The Ψ_s^c values calculated from the mean values of d and w in this study, however, were smaller than the measured mean values, Ψ_s^m. The measured median values, however, are significantly lower about 15° than those calculated from d/w.

Table 1. Groove widths and angles measured by AFM

Temp. (°C)	*t (h)*	*w (nm) average*	*Median standard error (W)*	d_{avg} *(nm)*	*Range of* Ψ*(deg)*	*Median standard error (cey)*	$\Psi^m{}_s$ *(deg)*	$\Psi^c{}_s$ *(deg)*
1370	1	264	±22·0	20	124–170	±3·95	153	140·3
	4	328	±11·3	28·5	126–167	±3·26	147·2	135
	10	396	±18·1	46·9	116–156	±2·93	141·8	121·2
	28	529	±36·2	49·1	120–164	±8·38	147·2	132·3
1450	1	377	±22·4	45	102–164	±3·87	138	120·8
	4	533	±41·8	65·5	112–157	±2·52	134·4	119·3
	10	710	±41·1	111·5	110–149	±2·49	122·7	106·7
	28	820	±47·8	179·4	104 135	±2·00	119·3	87·8
1530	1	712	±36·5	95·6	114–155	±3·06	130	114·8
	4	915	±52·1	110	120–151	±2·31	136·4	120·4
	10	1174	±53·3	203	96–140	±3·25	117·6	100·9
	28	1347	±72·4	222	79–137	±4·08	110·9	103·9
1600	1	1088	±42·6	153	100–153	±3·31	124·6	112·5
	4	1384	±76·5	192·3	98–151	±3·02	126·7	113·5
	10	1646	±93·2	309	81–131	±6·20	102·3	96·4

$\Psi^m{}_s$, measured mean value; $\Psi^c{}_s$, calculated by eqn (3) from average d/w ratio.

Table 2. Groove angles measured by various techniques

Material	Ψ_s^m	Ψ_s *range*	*Technique*	*Comments (w range:μm)*	*Reference*
Al_2O_3		114–159°	OI	faceted pores	9
MgO-doped Al_2O_3	139°	123–155°	OI	1273–1736K/3h	7
Al_2O_3	115°	85–170°	MRL	1873K/1h(0·5)	1
MgO-doped Al_2O_3	117°	85–170°	MRL	1873K/3h(2–4)	1
MgO-doped Al_2O_3	130°	114–140°	CRL	1673K/12h	2
Al_2O_3	130°	89–170°	AFM	1643–1873K(0·3–1·6)	This work

OI, optical interferometry; MRL, metal reference line method; CRM, carbon reference line method.

The measured Ψ_s increased with decreasing temperature or time. This is not an expected result and could come from the systematic errors of AFM (the tip artifacts). It is noted that the Ψ_s decreased slightly as the annealing time increased. This variation in Ψ_s with time is not a measurement error judging from the Ψ_s's of the grooves whose sizes are similar independent of the annealing temperature. In the case of very small grooves smaller than 400 nm, however, the accuracy of the angle becomes poor because the limitation comes from the size of the tip end, so we cannot discuss this one quantitatively. The assessment[8] of the probable errors in the measurement of Ψ_s requires that the measured Ψ values for a groove decrease and approache the actual values as the resolution of the technique increases or the groove width increases. These very small grooves would reflect some errors as this assessment. In our opinion, however, this variation of Ψ_s could tell that the initial groove profile can be different from the final shape, because these variation were observed also for large grooves which are enough large not to make error from the AFM tip size problem.

As the temperature increased, the Ψ_s also became smaller. This could be understood by considering the possibility that the entropy term of the surface energy would be larger than that of the grain-boundary energy, i.e. the surface energy depends more on temperature than grain-boundary energy does, so that the Ψ decreases as the temperature increases. The dihedral angles measured in this work are compared with the reported values in Table 2. The values depend on the sample purity and possibly on the measuring technique.

3.3 Surface diffusion coefficient

The groove width, w, was measured as a function of time and temperature (Table 1). Fig. 5 shows w versus $t^{1/4}$ plots for each temperature according to eqn (1). All data points lie on a straight line for all temperatures which firmly indicate that the

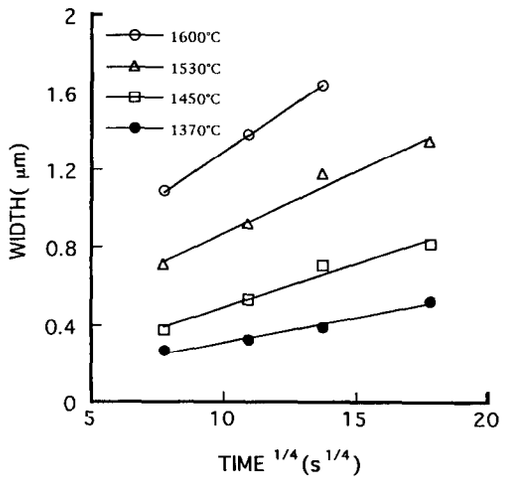

Fig. 5. Time dependence of the groove width at different temperatures.

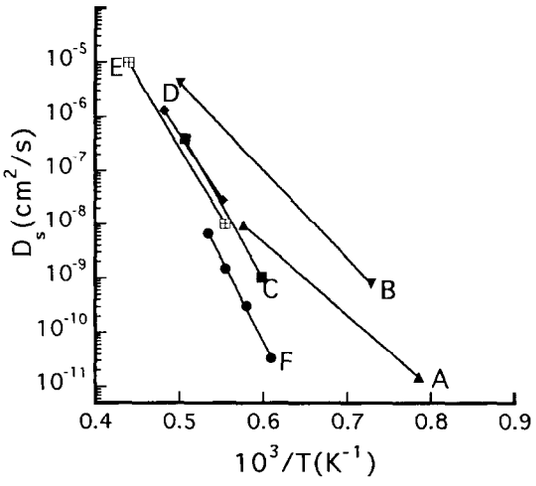

Fig. 6. Surface diffusion coefficient versus temperature. Alphabetical symbols correspond to those listed in Table 4.

Table 3. Parameters to calculate the surface diffusion coefficient

Temperature (°C)	$B^{1/4}$ $(\times 10^{-7}\ cm/s^{1/4})$	σ_{sv} $(\times 10^{-4}\ J\,cm^{-2})$	kT $(\times 10^{-20}\ J)$	$D_s(\times 10^{-10}\ cm^2\,s^{-1})$
1600	20·12	1·091	2·59	66·6
1530	14·09	1·145	2·50	14·8
1450	9·789	1·210	2·38	3·10
1370	5·733	1·271	2·27	0·331

Table 4. Parameters for surface diffusion measured from developing grooves

Symbol	*Material and purity*	*Technique*	*Temperature (K)*	D_o	Q_s kJ mol^{-1}	*Reference*
A	Sintered polycrystal 99·7%	Grain boundary groove, OI	1273–1736	0·48	256	5
B	Sintered polycrystal 99·7%	Grain boundary groove, OI	1373–1993	7×10^2	314	1
C	High purity single crystal	Grain boundary groove, OI	1673–1973	10^8	544	2
D	Bicrystal	Symmetric tilt grain boundary groove, OI	1813–2073	5×10^5	460	10
E	High purity single crystal	Grain boundary groove, OI	1773–2273	$4{\cdot}05\times10^5$	452	4
F	Sintered polycrystal 99·7%	Grain boundary groove, AFM	1643–1873	$8{\cdot}22\times10^7$	577	This work

grain-boundary grooving takes place via surface diffusion. This result is in accordance with other researchers' reports.

The slope of each line is equal to 4·6 $B^{1/4}$ and the surface diffusion coefficient can be calculated using eqn (2). Table 3 presents the experimental parameters (from Ref. 11) and the calculated D_s for different temperatures. The resulting D_s values are plotted in Fig. 6 along with the results of other researchers. The surface diffusion coefficient obtained in the present study can be expressed as: $D_s = D_o \exp(-Q_s/RT) = 8{\cdot}22\times10^7\times\exp[-1577\pm30$ (kJ mol^{-1})/RT]cm^2 s^{-1}. In Table 4 are summarized the values of D_o and Q_s reported in the literature which were all obtained by the grain-boundary grooving method. The differences in the reported D_s are probably due to the choice of different materials and different annealing temperature ranges.

Lines A and B in Fig. 6 clearly fall in a different region with the activation energy about 50% lower than others and their absolute values about an order of magnitude greater. Higher values of D_s with lower activation energies can be attributed to the effect of defects introduced during surface polishing.[1,5] Lines C, D and E are substantially similar with high activation energies indicating the so-called intrinsic surface diffusion having taken place.

Line F is the one obtained in this study. The D_s is about an order of magnitude smaller and the Q_s is about 10% higher than other values. Why much smaller values of D_s were obtained, however, is difficult to understand. A possible explanation is that the ambipolar diffusion takes place on the surface in a way which is far from ideal due to the microstructure where large grains with few tens of μm and small grains with a few μm in size are coexisting. Mass transport should simultaneously occur along diffusion paths other than surfaces because grain growth never fails to take place in heterogeneous microstructure with larger grains consuming smaller grains even during annealing, and this complexity in mass transport must have affected the accuracy of the data analysis.

The effect of impurities on the grain-boundary grooving was first investigated in the work of line C.[2] The effect of the addition of impurities, however, was somewhat ambiguous, and there is no clear answer yet. On the other hand, the beneficial effect of addition of MgO in the sintering of alumina was discovered several decades ago,[12] and MgO addition is said to keep the surface free from Ca and other impurities,[13] or to make the surface layer negatively charged.[14] This type of impurity effect could also affect the surface diffusivity.

4 Summary

A series of polycrystalline alumina was annealed at 1370~1600°C in air to develop the grain-boundary grooves, and they were observed by AFM which could measure very small grooves with high accuracy. The measured groove angle and the ratio of grain-boundary energy to surface energy slightly varied with annealing temperature and time giving the mean values of 130·1° and 0·855, respectively, at 1370~1600°C. The grain-boundary grooving was proved to be surface diffusion controlled and the surface diffusion coefficient was obtained as $D_s = D_o\exp(-Q_s/RT)$ with $D_o = 8{\cdot}22\times10^7$ cm^2 s^{-1} and $Q_s = 577\pm30$ kJ mol^{-1}.

Some problems to be solved in this method using AFM are discussed but recent development on the tips, for instance sharpened tip made by outgrowing, could reduce the measurement errors and enable us to measure the samples of very fine grain size which is difficult to observe using other methods.

References

1. Robertson, W. M. and Chang, R., The kinetics of grain-boundary groove growth on alumina surfaces. In *Materials Science Research, Vol 3. The Role of Grain Boundaries and Surfaces in Ceramics*, ed. W. W. Kriegel and H. Palmour III. Plenum Press, New York, 1966.
2. Robertson, W. M. and Ekstrom, F. E., Impurity effects in surface diffusion on aluminium oxide. In *Materials Science Research Vol. 4. Kinetics of Reactions in Ionic Systems*, ed. T. J. Gray and V. D. Frechette. Plenum Press, New York, 1969.
3. Handwerker, C. A., Dynys, J. M., Cannon, R. M. and Coble, R. L., Dihedral angles in magnesia and alumina: distribution from surface thermal grooves. *J. Am. Ceram. Soc.*, 1990, **73**(5), 371–77.
4. Gaddipati, A. R. and Scott, W. D., Surface mass transport of alumina. *J. Mater. Sci.*, 1986, **21**, 419–423.

5. Tsoga, A. and Nikolopoulos, P., Groove angles and surface mass transport in polycrystalline alumina. *J. Am. Ceram. Soc.*, 1994, **77**(4), 954–960.
6. Mullins, W. W., Theory of thermal grooving. *J. Appl. Phys.*, 1957, **28**(3), 333–339.
7. The operating manual of AFM used in this work; model SFA300 made by Seiko Electronic. Co., chapter 6., 1994.
8. Handwerker, C. A., Dynys, J. M., Cannon, R. M. and Coble, R. L., Metal reference line technique for obtaining dihedral angles from surface thermal grooves. *J. Am. Ceram. Soc.*, 1990, **73**(5), 1365–1371.
9. Schwarz, U. D., Haefke, H., Reimann, P. and Gunterodt, H., Tip artefacts in scanning force microscopy. *J. Microscopy*, 1994, **173**(3), 183–197.
10. Shackelford, J. F. and Scott, W. D., Relative energy of [1100] tilt boundaries in aluminum oxide. *J. Am. Ceram. Soc.*, 1968, **51**(12), 688–692.
11. Nikolopoulos, P., Surface, grain-boundary, and interfacial energies in Al_2O_3 and Al_2O_3-Sn, Al_2O_3-Co Systems. *J. Mater. Sci.*, 1985, **20**, 3993–4000.
12. Coble, R. L., Song, H., Brook, R. J., Handwerker, C. A. and Dynys, J. M., Sintering and grain growth in alumina and magnesia. In *Advances in Ceramics*, Vol 10, ed. W. D. Kingery. The American Ceramic Society, Columbus, OH, 1984.
13. Mukhopadhyay, S. M., Jardine, A. P., Blakely, J. M. and Baik, S., Segregation of magnesium and calcium to the (1010) prismatic surface of magnesium implanted sapphire. *J. Am. Ceram. Soc.*, 1988, **71**(5), 358–362.
14. Baik, S., Fowler, D. E., Blakely, J. M. and Raj, R., Segregation of Mg to the (0001) surface of doped sapphire. *J. Am. Ceram. Soc.*, 1985, **68**(5), 281–286.